Translational and Rotational Motion of C8 Aromatics Adsorbed in Isotropic Porous Media (MOF-5): NMR Studies and MD Simulations

Velencia J. Witherspoon,[†] Lucy M. Yu,[†] Sudi Jawahery,[†] Efrem Braun,[†] Seyed Mohamad Moosavi,[‡] Sondre K. Schnell,[¶] Berend Smit,[‡,†] and Jeffrey A. Reimer[*,†,§]

†*Department of Chemical and Biomolecular Engineering, University of California, Berkeley, Berkeley, CA 94720, USA*

‡*Institut des Sciences et Ingénierie Chimiques, Valais, École Polytechnique Fédérale de Lausanne (EPFL), Rue de l'Industrie 17, CH-1951 Sion, Switzerland*

¶*Department of Materials Science and Engineering, Norwegian University of Science and Technology, 7491, Trondheim, Norway*

§*Materials Science Division, Lawrence Berkeley National Laboratory, Berkeley, California, 94720, USA*

E-mail: reimer@berkeley.edu

Abstract

We combined nuclear magnetic resonance (NMR) and molecular dynamics (MD) simulation to study xylene behavior in MOF-5, probing the effects of adsorbate geometry in a weakly interacting model isotropic metal-organic framework (MOF) system. We employed NMR diffusometry and relaxometry techniques at low field (13 MHz) to quantify the self-diffusion coefficients (D_s) and the longitudinal relaxation times (T_1) of xylenes in MOF-5 as a function of temperature at the saturated loading for each xylene. These experiments reveal the translational motion activation energies to be 15.3, 19.7, and 21.2 kJ mol^{-1} and the rotational activation energies to be 47.26, 12.88, and 11.55 for the (p-,m-,o-) xylene isomers respectively. Paraxylene exhibits faster translational motion, yet shows four times the activation energy barrier for rotational motion vis-à-vis the other isomers. MD simulations performed on these model systems corroborate the findings for paraxylene and suggest that paraxylene has the lower free energy barrier for hopping away from its binding sites, yet has the slowest rotational motion in the plane of the xylene molecule.

Introduction

MOFs are a type of porous media under investigation for applications that require molecular specificity.[1] Since the initial discovery of MOF-5 (also known as IRMOF-1),[2] this novel class of materials has been explored for potential use in gas separation and storage, selective catalysis, and numerous other industrial applications. Targeted design and synthesis[3] enables modularity in MOFs achieving highly desired adsorbent characteristics.[4,5] More recently, MOFs have been investigated for many liquid separation processes that require a distinctive difference in the transport behavior of small molecules.[6]

To determine the suitability of these adsorbents for particular applications, transport phe-

nomena are commonly investigated by performing macroscopic measurements (e.g. breakthrough measurements) that characterize effective mass transport values containing contributions from both the intercrystalline and the intracrystalline regimes.[7] To gain insight into the mechanisms that determine these macroscopic measurements, molecular-scale interactions need to be measured. In particular, MOFs offer the nanoporous media community a unique opportunity to improve our understanding of how adsorbed molecules move in a confined spaces since both the topology and the chemical affinity is well-defined.[8] Although MD simulations have been instrumental in developing a physical description of adsorbate motion in porous media, there are very few experimental studies on motional dynamics of the adsorbed molecules that can be used to validate these findings.

Many researchers employ NMR-based techniques to quantify the self-diffusion coefficients in an effort to understand translational motion. The NMR longitudinal relaxation times are analogous to the self-diffusion coefficients,[9] in quantifying rotational motion of adsorbates in MOF systems.[10–13] Most of these studies have focused on determining differences between strongly and weakly adsorbed molecules, where stark differences in the observed self-diffusion coefficient and longitudinal relaxation time are used to understand motion and selectivity.[12,13]

The separation of xylene isomers poses a lucrative scientific challenge, as a distillation of these isomers accounts for a significant amount of global energy consumption.[14] Composed of a conjugated ring perturbated by two methyl groups, xylene isomers have similar kinetic diameters (less than 1 Å differences) and similar chemical interaction energies which make the design of a selective adsorbent difficult. The selectivity of MOFs such as MIL-47[15–17] and MIL-53[18–21] for xylene isomers has been studied and attributed slectivity to framework anisotropy that affects π-π stacking, which was identified as the dominant type of host-guest interaction. Macroscopic breakthrough measurements at high temperature (553 K) and pressure (1.2 bar) were used to determine transport intracrystalline diffusivities of xylenes in MOF-5 and showed that the vapor phase paraxylene diffused two times slower than the other isomers.[22] Previous descriptions of how C8 aromatics diffuse in a porous environment postulate that entropy may play a greater role in determining the molecular mobility,[23–26] yet present very little systematic experimental evidence.

We have chosen to employ magnetic resonance methods to quantify D_s as a characterization of translational motion and NMR relaxometry to probe the local rotational motion of adsorbed xylene isomers in the MOF-5 framework. We explore how subtle geometric differences in the xylene isomers are manifest in translational and rotational motion. To further analyze the interplay between rotational and translational motion, we conduct MD simulations to calculate D_s, spatial probability distributions, rotational diffusion coefficients, and relative orientations of the xylene isomers in MOF-5.

Methods

MOF-5 Synthesis and Characterization

MOF-5 was synthesized by preparing a 3:1 mixture of zinc nitrate hexahydrate and 1,4-benzenedicarboxylic acid (Sigma Aldrich chemicals, 99.95 % purity) in 100 mL of diethylformamide (DEF) and heating for 72 hours at 90 °C, resulting in a typical crystal size of 425 µm. Solvent exchanges from DEF to dry dimethylformamide (DMF) were followed by solvent exchanges from DMF to dry dichloromethane (DCM) in preparation for activation. After solvent exchange, powder x-ray diffraction spectra were measured at room temperature using a D8 Discover GADDS Powder XRD (see Supporting Information)) and nitrogen (Praxair, 99.999 %) adsorption isotherms were collected using a Micromeritics TriStar 3000 BET instrument determined the BET surface area of the crystals to be 3,565 $m^2\,g^{-1}$. A flow of argon gas at a temperature of 150 °C degassed the samples overnight. Afterwards a 425 µm sieve separated approximately 100 mg

of the larger crystals, which were activated overnight at 150 °C and 0.001 mbar of vacuum in a flame-dried 5 mm glass NMR tube.

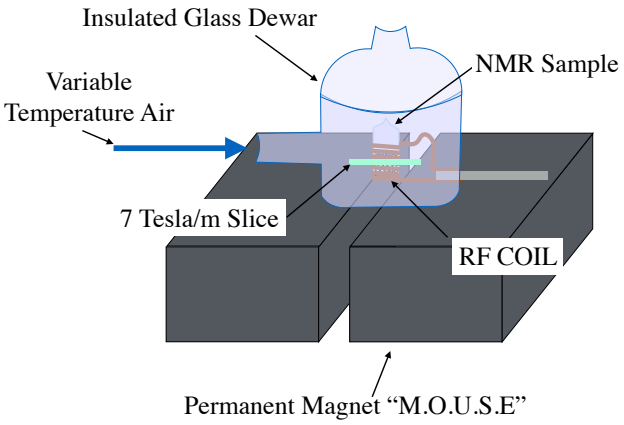

Figure 1: A schematic representing the custom homebuilt probe and temperature control setup used to make measurements. A volumetric coil is centered in the 1 mm selective slice inherent to xylene. A glass dewar was placed on top of the permanent magnet and was used to insulate the sample and electronics from the environment.

Ex-Situ NMR Preparation and Measurements

After activation, the sample was dosed with a predetermined microliter amount of high purity degassed anhydrous xylenes purchased from Sigma Aldrich. NMR spin counting methods (7.4 T magnet using a Tecmag Discovery Magnet with a 5 mm Solid State NMR MAS Doty probe), as well as gravimetric methods, yielded loadings of (49 to 56 molecules/unit cell) for each xylene isomer. These loadings ensure that all adsorbed xylene molecules were in the high-density liquid-like phase based on theoretically-determined vapor-liquid phase diagrams provided previously.[27] The samples were flame sealed using a cold bath and liquid nitrogen, giving a minimal headspace of approximately 0.018 cm^3. The linear strayfield of a 0.3 T single sided magnet[28] equipped with a temperature controlling dewar was used for all NMR experiments (Fig. 1). The magnet field gradient strength was confirmed to be 7 T m^{-1} through liquid diffusion calibrations. In order to increase sensitivity we constructed a home built probe using a solenoid copper coil oriented perpendicularly to the magnetic field direction, combined with a remote tuning box (Fig. 1). A Magritek Kea II Spectrometer was used with Prospa® operating software for the data acquisition. Power modulation was used to control the pulsed angle during all experiments.

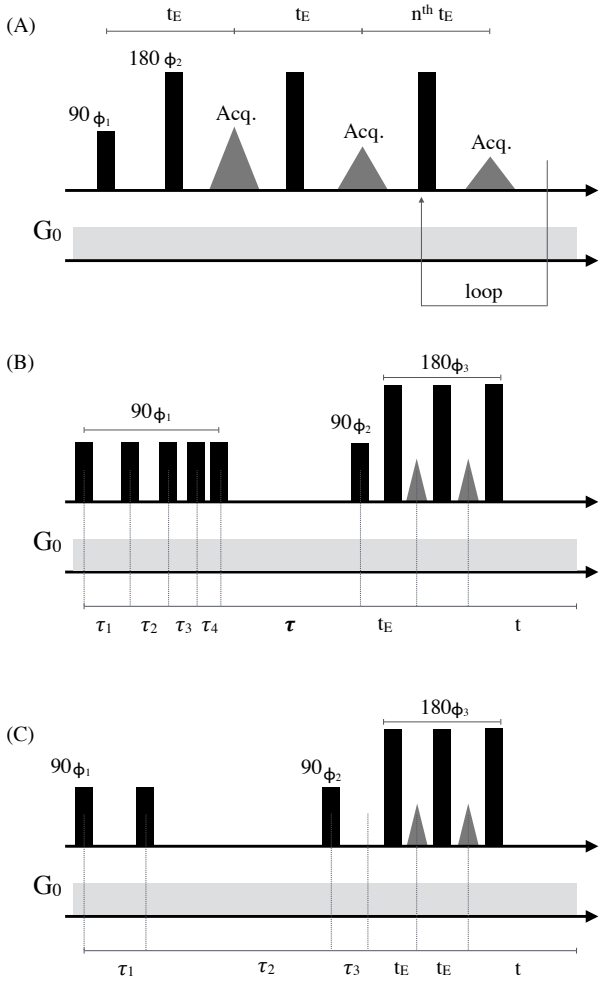

Figure 2: The standard NMR schematic for (A) the Carr-Purcell-Meiboom-Gill (CPMG) pulse sequence, (B) the Saturation Recovery pulse sequence with CPMG acquisition for inhomogeneous fields and (C) the Stimulated Echo sequences with CPMG acquisition for inhomogeneous fields.

The CPMG sequence[29] was used to measure the transverse relaxation time (T_2), as shown in Fig. 2A. Further basic pulse sequences employed a CPMG acquisition train. The Satu-

ration Recovery pulse sequence (Fig. 2B) was used to measure the longitudinal relaxation time constant, T_1. A constant gradient stimulated echo (STE) pulse sequence with a CPMG acquisition and phase tables[30] (Fig. 2C) were used to determine the apparent D_s. These were interpreted as the intracrystalline diffusivities due to the large crystal size (450 µm) and small diffusion time, τ_2, (10 to 100 ms) chosen. This sequence has been shown to minimize decoherence of the signal due to transverse relaxation by storing the signal along the z-axis during the experimental diffusion time. During this storage interval, the signal experiences negligible longitudinal relaxation. The resulting signal was T_2-corrected during post-processing for the transverse relaxation experienced during the intervals of τ_1 and τ_3. The signal intensity as a function of τ_1 was analyzed using Numerical Non-Negative Linear "Inverse" Laplace Transformation (NNL) with Tikhonov regularization to yield a spectrum of self-diffusion coefficients.[30,31] This algorithm was provided with the Prospa® software from Magritek.

Molecular Dynamics Simulation Details

Molecular dynamics simulations were conducted with LAMMPS[32] in the NVT ensemble using a timestep of 0.5 fs, the Nosé-Hoover chain thermostat[33,34] and a rigid-body time integrator.[35] The Lennard-Jones potential, shifted and truncated at 12.0 Å, was used to describe dispersive interactions. Framework atoms were modeled with a previously published force field,[36] adsorbate molecules were modeled with the TraPPE force field,[37] and Lorentz-Berthelot mixing rules were used to calculate cross-interactions; this force field has been shown to provide good agreement with experimental diffusion coefficients of small aromatic molecules in MOF-5.[36] As the TraPPE models do not have partial charges, Coulombic interactions were not calculated. The framework was assumed to be rigid since it has been shown[38] that framework flexibility does not have an effect on adsorbate diffusion in MOF-5. and the experimental crystal structure[39] was used.

The frameworks were loaded with guest molecules at densities corresponding to the saturated liquid densities found by simulations in a previous study.[27] These densities are shown in Table 1, below. The periodic simulation box comprised 1 unit cell of MOF-5, (cubic with a 25.832 Å side length).

Table 1: Loadings used in the MD simulations in units of molecules per unit cell.

Temperature (K)	o-xylene	m-xylene	p-xylene
270	54	53	53
280	53	53	53
290	53	51	51
300	52	50	50

All MD simulations were equilibrated for 5 ns, followed by a production period of at least 100 ns, which was found to be sufficiently long for the mean-squared displacement (MSD) to become a linear function of time, as verified by measuring the slope of the MSD plot on a log-log scale. Self-diffusion coefficients were obtained by fitting the Einstein relation, $D_s = \frac{1}{6}\lim_{t\to\infty}\frac{d}{dt}\left\langle[r(t)-r(0)]^2\right\rangle$, to the linear portion of the MSD versus time plot, using the order-n algorithm[40,41] to collect MSD data.

Rotational Calculation of Spatial and Orientational Probability Distributions

Spatial density distributions of xylenes were generated from MD simulations (Fig. 3), where the center-of-mass of each xylene molecule was recorded every 5 fs and binned into a $100 \times 100 \times 100$ grid overlaid on the MOF-5 structure. As MOF-5 is cubic, the three-dimensional grid was reduced to a two-dimensional grid by averaging together all slices in one of the dimensions. In Fig. 3 these data are presented in the form of a probability maps. The angle between methyl groups on xylene molecules and the nearest neighboring carboxylate group was recorded every 0.5 ps. The methyl bond vector was defined as pointing from the aromatic carbon atom on the xylene to its bonded united atom methyl group. The carboxylate bond vector was defined as having either the carboxylate oxygen or carboxylate carbon as its vertex such

that the vector always pointed in the positive x, y or z direction. These definitions yield symmetric distributions of the calculated angle. In Fig. 4, these data are presented in the form of probability density functions.

Rotational Diffusion Coefficient Calculations

We define rotational displacement as $\hat{\psi}(t) = \int_0^t \Delta\hat{\psi}(t')dt'$ where both the magnitude and direction of vector $\Delta\hat{\psi}(t')$ are given by the normalized vector of interest $u(t)$ at times $t = t',t' + dt'$. The magnitude of $\Delta\hat{\psi}(t')$ is given by $|\Delta\hat{\psi}(t')| = \cos^{-1}\left(u(t' + dt') \cdot u(t')\right)$ and direction is given by $u(t' + dt') \times u(t')$.[42] In this work, the vector of interest $u(t)$ is either the bond vector pointing from an aromatic xylene ring carbon to the its bonded methyl group (in-plane, $\parallel$) or the vector normal to the aromatic xylene ring (out-of-plane, $\perp$).

Analogously to translational motion, rotational self-diffusion coefficients were obtained by fitting the relation, $D_r = \frac{1}{4}\lim_{t\to\infty}\frac{d}{dt}\left\langle\left[\hat{\psi}(t) - \hat{\psi}(0)\right]^2\right\rangle$ to the linear portion of the rotational MSD versus time plot, defined as $\langle\psi^2(\Delta t)\rangle = \left\langle\left[\hat{\psi}(t + \Delta t) - \hat{\psi}(t)\right]^2\right\rangle$.

Results and discussion

Translational Motion

The self-diffusion coefficients of (*p,m,o*)-xylene were measured as a function of diffusion time (τ_2) ranging from 10 to 100 ms, and temperatures ranging from 253 to 293 K. These diffusion times were chosen to ensure that the xylene molecules would spend most of their time sampling the intracrystalline environment belonging to MOF-5 and very little time experiencing the inter-crystalline environment. The characteristic length (l_D) traveled by the adsorbed molecule was estimated using $l_D = \sqrt{D_{app}\tau_2}$; varying diffusion times from 10 to 100 ms yielded a range of characteristic lengths from 100 to 0.1 µm, much smaller than the MOF-5 crystal size. None of the self-diffusion coefficients of the xylene isomers demonstrated a strong dependence on the diffusion time, τ_2 (see Supporting Information). All self-diffusion coefficients of the xylene isomers were dependent on the temperature and were analyzed with an Arrhenius fit of the self-diffusion coefficients at the shortest τ_2 value (10 ms). In this way the values of translational activation energy ($E_{a,\mathrm{trans}}$) and the entropic pre-exponential coefficient ($D_{0,\mathrm{trans}}$) of the xylene isomers were determined (Fig 5 and Table 2).

Paraxylene displays the fastest experimentally-determined self-diffusion coefficients at all temperatures (Fig. 5) and the lowest experimental calculated activation energy for translational motion (Table 2). Paraxylene translational motion in MOF–5 deviates from bulk isomer behavioral trends[43] by exhibiting the smallest pre-exponential factor; this is surprising because when measured in bulk it has the largest.[44] The simulated D_s are on the same order of magnitude as the experiment and display the same ordering between isomers. However, the temperature dependence of the simulated D_s do not compare well with experiment, which is likely due to the D_s being very sensitive to adsorbate loadings, the temperature dependence of which could only be estimated based on past simulation work (Table 1).

We further explored the guest molecule configurations by considering the spatial probability distributions from the MD simulations (Fig. 3). These figures reveal the preferential adsorption sites of each xylene isomer. Metaxylene prefers to adsorb in the center of the pore, while orthoxylene prefers adsorption closer to those metal clusters that are located at the corners of the pore (Fig. 3 A and B, darker shaded areas). Paraxylene, by contrast, shows a more uniform distribution (Fig. 3 C). The presence of multiple and proximal preferential adsorption sites for orthoxylene and metaxylene suggests that their translational diffusion mechanism involves the hopping of molecules between these sites and that these adsorbates must overcome a larger free energy barrier to translate compared to paraxylene. These observations are consistent with the trend in the experimentally determined translational activation energies.

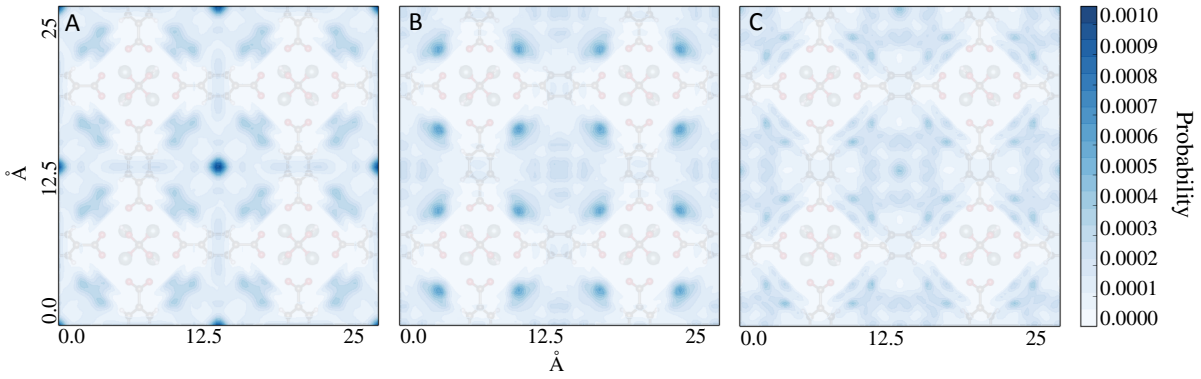

Figure 3: Results of the MD simulations at 280 K and loadings are shown in Table 1 displaying the spatial probability distribution of liquid phase xylene molecules in the MOF-5 structure: (A) metaxylene, (B) orthoxylene, (C) paraxylene.

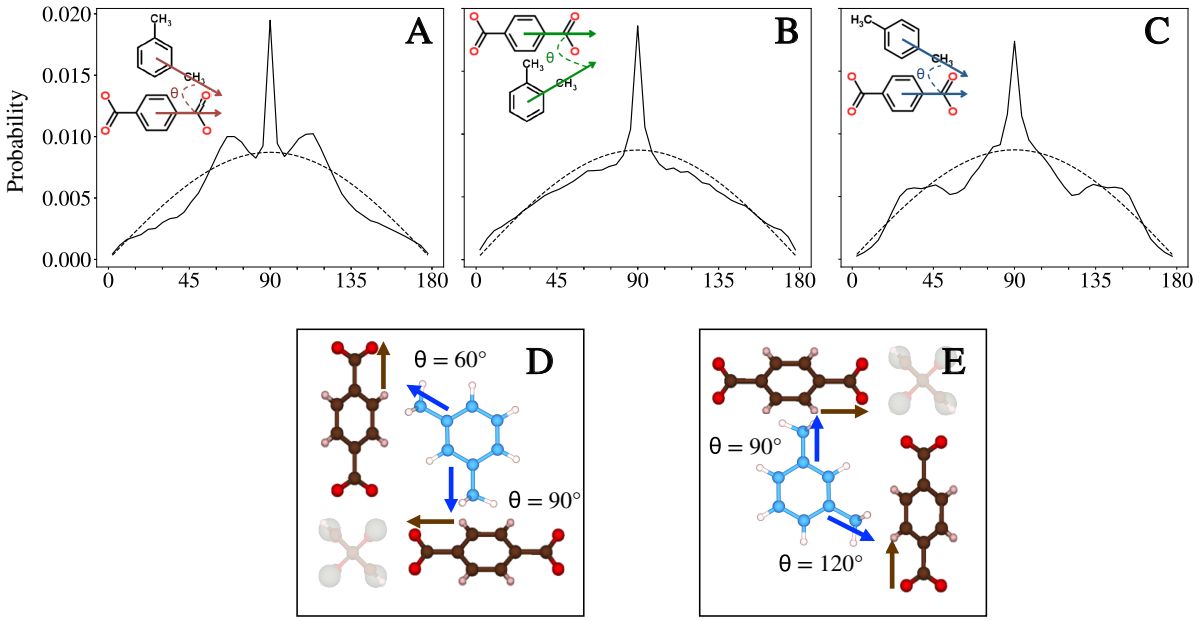

Figure 4: Probability density functions describing the likelihood of finding a methyl bond on a xylene molecule oriented at a range of angles relative to the nearest neighboring carboxylate group on a framework linker, demonstrated by (D) and (E), and the resulting distributions (A) metaxylene, (B) orthoxylene, (C) paraxylene. In (A), (B) and (C), the dashed black lines reflect a random distribution of methyl orientations. In (D) and (E), oxygen atoms are red, hydrogen atoms are light pink and carbon atoms on the xylene and linker are blue and brown, respectively.

Rotational Motion

The standard expression of the spin-lattice relaxation rate as a result of homonuclear dipolar coupling is $R_1 \propto J(\omega) + 4J(2\omega)$,[45,46] where R_1 is the inverse of T_1, J is the spectral density function, and ω is the Larmor frequency. We employ the simplified Lipari-Szabo model[47,48] as the descriptor for the spectral density function to separate the contributions of molecular rotational motion and internal methyl motions to R_1. In this model-free formalism the spectral density is related to the correlation times by the expression, $J(\omega) = \frac{2}{5}\frac{\tau_m S^2}{1+\omega^2\tau_m^2} + \frac{(1-S^2)\tau}{1+[\tau^2\omega]^2}$, where τ_m is the isotropic rotational correlation time of the molecule, $\tau = \frac{\tau_m\tau_e}{\tau_m+\tau_e}$, and τ_e is an effective correlation time for internal motions (associated

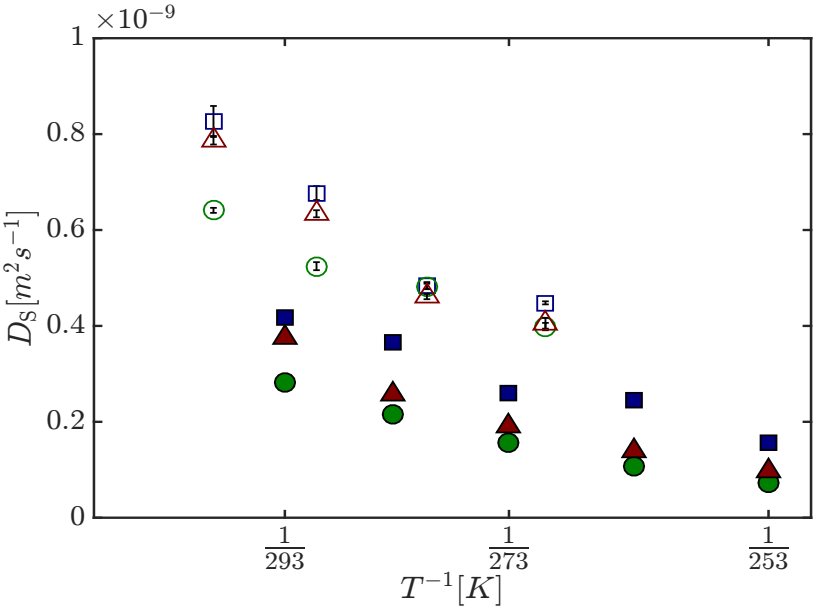

Figure 5: A plot of the experimental inverse temperature dependence of the self-diffusion coefficient for each xylene (para ■ , ortho ●, meta ▲) isomer at constant loading of 6 to 7 molecules/cage, and the simulated self-diffusion coefficients, (para □, ortho ◯, meta △).All error is calculated as the standard deviation of the measurement and is contained within the demarcation.

Table 2: Translational activation energy ($E_{a,\mathbf{trans}}$) calculated from an Arrhenius fit to the experimental data and simulated data from Fig. 5. The actual $D_{0,\mathbf{trans}}$ were taken from the intercept of the linear fit with inverse temperature.

	p-xylene	m-xylene	o-xylene	
Experimental	$E_{a,trans}$ (kJ mol^{-1})	15.3	19.7	21.2
$D_{0,\mathrm{trans}}$ (m^2 s^{-1})	1.8 $\times 10^{-7}$	1.68 $\times 10^{-6}$	2.45 $\times 10^{-6}$	
Simulated	$E_{a,trans}$ (kJ mol^{-1})	15.3	16.1	10.3
$D_{0,\mathrm{trans}}$ (m^2 s^{-1})	3.79 $\times 10^{-7}$	3.93 $\times 10^{-8}$	5.06 $\times 10^{-7}$	

with methyl groups for xylene isomers); S^2 is a generalized order parameter ranging from 0 to 1 representing the degree of spatial restriction of the molecule in a medium.[46]

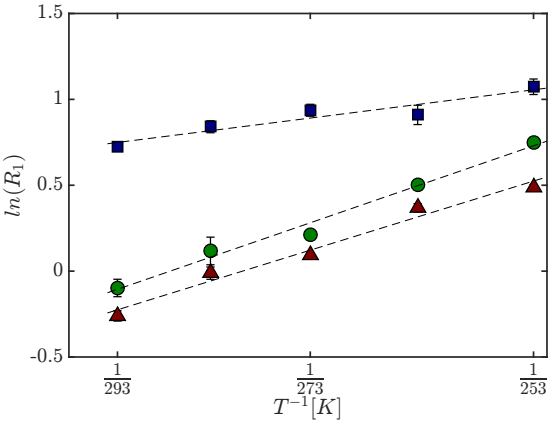

Figure 6: A plot of the experimental inverse temperature dependence of R_1 for each xylene (para ■ , ortho ●, meta ▲) isomer at constant loading of 6 to 7 molecules/cage.

Under the conditions in which the internal motion of methyl groups is extremely fast,[49] $\tau_e \ll \tau_m$, and the order parameter is large, the truncated form of the Lipari-Szabo spectral density function is suitable and internal motions (second additive terms) are neglected. The extreme motional narrowing regime applies, making it appropriate to associate $R_1 \propto S^2\tau_m$, assume the correlation time is exponential, then employ an Arrhenius analysis to determine the activation energies for restricted rotational motion of the xylenes adsorbed in MOF-5 (see Figure 6 and Table 3). Paraxylene is found to have almost four times the rotational activation energy of the other isomers and thus experiences some combination of increased spatial restriction (higher S^2 value) and/or a longer isotropic rotational correlation time. This is different from bulk behavior where the rotational activation energy ($E_{a,rot}$) were all on the same order of magnitude.[50]

MD simulations were performed at the aforementioned loadings and affirm the notion of paraxylene restricted rotational motion. For all three xylenes, two types of rotational motion were distinguished and tracked during the course of MD simulations. In-plane xylene rotation was tracked with the methyl bond vectors as a reference, and out-of-plane xylene rotation was tracked with the vector normal to the aromatic ring as a reference. Paraxylene displays a large difference between the in-plane and out-of-plane diffusion coefficients, with the out-of-plane coefficients being a factor of three larger (Fig. 7). The trend in the in-plane activation energies derived from these simulations show that paraxylene's activation energy is greater than that of both metaxylene and orthoxylene (Table 4).

Table 3: Experimental Rotational activation energy ($E_{a,\mathbf{rot}}$) of xylene molecules calculated from fitting the experimental longitudinal relaxation rate to an Arrhenius relation given in Fig. 6.

($\mathrm{kJ\,mol^{-1}}$)	p-xylene	m-xylene	o-xylene
$E_{a,rot}$	47.26	12.88	11.55

Table 4: The simulated in-plane and out-of-plane rotational activation energies and the pre-exponential factors fitted from an Arrhenius relation in Fig. 7.

	para	meta	ortho
$E_{a,rot,\parallel}$ ($\mathrm{kJ\,mol^{-1}}$)	17.03	11.37	6.0
$D_{0,\mathrm{rot},\parallel}$ ($\mathrm{rad^2\,ps^{-1}}$)	37.83	5.95	1.4
$E_{a,rot,\perp}$ ($\mathrm{kJ\,mol^{-1}}$)	10.84	10.06	9.05
$D_{0,\mathrm{rot},\perp}$ ($\mathrm{rad^2\,ps^{-1}}$)	10.43	4.2	2.44

To further explore the effect of confinement on the orientations sampled during rotational motion, the angle between the methyl bond and the bond connecting the nearest-neighbor carboxylate group to the aromatic part of organic linker was tracked. The probability of finding a molecule oriented at a particular angle was then calculated for each xylene and the results are displayed in Fig. 4. The observed probability distributions shown in solid black lines can be compared to the dashed black lines, which shows a random distribution of methyl group orientations with the functional form $P(\theta) = \frac{1}{2}\sin(\theta)$. All xylenes display a dominating peak larger than that of the random distribution around 90°. This suggests the

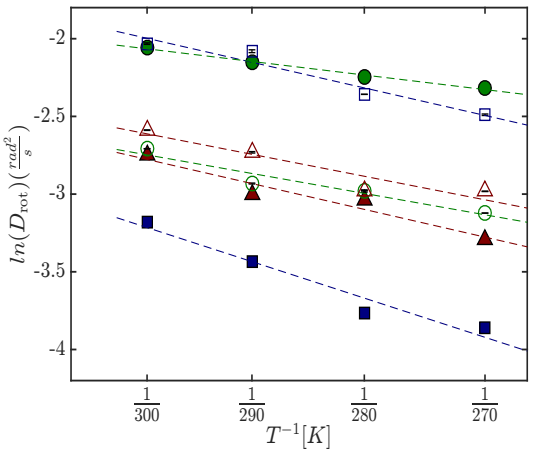

Figure 7: The inverse temperature dependence of the simulated rotational self diffusion coefficients for each xylene isomer at constant loading, where the filled symbols represent the in-plane rotation,(para ■ , ortho ●, meta ▲), results and the empty symbols represent the out-of-plane results, (para □, ortho ◯, meta △). The dashed lines represent the linear fit for an Arrhenius relationship.

most favored orientation for a methyl group relative to the framework phenyl ring may be a *t*-configuration near π-pocket of the ligand. This is not the case for orthoxylene, as Fig. 3 shows that the molecular center-of-mass is predominantly found in the corners of the pore rather than the center.

Additional features in the metaxylene and paraxylene angle probability distributions can be intuited by considering the positions of the two methyl groups relative to each other. Fig 4 c and d demonstrate the proposed metaxylene configurations. The peaks at 60° and 120° in the metaxylene plot are observed because when one methyl group is in the favored orientation (perpendicular to one set of linkers) and the aromatic xylene ring is parallel to the other set of organic linkers, the second methyl group forms a 60° or 120° angle with the nearest neighboring carboxylate group. The paraxylene distribution is unique because when the aromatic xylene ring is similarly-aligned parallel to one set of organic linkers, both methyl groups would be perpendicular to the other set, and there would be only a single peak at 90°. The additional features at 140° and 40° indicate that paraxylene cannot fit into configurations where it is oriented exactly parallel to a set of organic linkers and must be tilted with respect to the pore. Paraxylene therefore samples a more restrictive environment due to its rigid rod like shape.

Conclusion

MOF-5, synthesized as a large crystal, was imbibed with saturated-liquid loadings of metaxylene, orthoxylene, and paraxylene. The effects of subtle geometric differences between the isomers were manifest in the guest molecule translational and rotational motions, as observed using NMR techniques. The quantification of the self-diffusion coefficient and the longitudinal relaxation time as functions of temperature at constant loading allowed for the quantification of the translational and rotational activation energies for each species. Paraxylene was experimentally observed to have the fastest self-diffusion coefficient at all temperatures (p>m>o), the lowest activation energy for translational motion (p<m<o), and the highest activation energy for rotational motion (p>m>o). These results were compared with MD simulations and confirm the constriction of rotational freedom in an isotropically confined geometry and the faster translational motion of the most rod-like molecule, paraxylene. MD simulations indicate that neither metaxylene nor orthoxylene experienced comparable restrictions for in-plane rotations when adsorbed in MOF-5, supporting the experimental findings that paraxylene faces higher energy barriers for rotational motion.

Acknowledgement This work was supported as part of the Center for Gas Separations Relevant to Clean Energy Technologies, as an Energy Frontier Research Center funded by the U.S. Department of Energy, Office of Science, Basic Energy Sciences under Award DE-SC0001015 (Experimental and Characterization studies), by the National Science Foundation under Award DGE 1106400 (stipend VW, SJ), SKS acknowledge ENERSENSE (Grant

Number 68024013) for financial support, and this research used resources of the National Energy Research Scientific Computing Center, a DOE Office of Science User Facility supported by the Office of Science of the U.S. Department of Energy under the Contract No. DE-AC02-05CH11231.S.M.M. was supported by the Deutsche Forschungsgemeinschaft (DFG), priority program SPP 1570 and SKS acknowledges Sigma2 (project NN9414K) for computational resources. We acknowledge Douglas Reed from the lab of Prof. Jeffrey Long at UC Berkeley for measurement of the adsorption isotherms at room temperature.

Supporting Information Available

References

(1) Rowsell, J. L.; Yaghi, O. M. Metal-organic frameworks: a new class of porous materials. *Microporous Mesoporous Mater.* **2004**, *73*, 3–14.

(2) Li, H.; Eddaoudi, M.; O'Keeffe, M.; Yaghi, O. Design and synthesis of an exceptionally stable and highly porous meatal organic frameworks. *Nature* **1999**, *402*, 276–279.

(3) James, S. L. Metal-organic frameworks. *Chem. Soc. Rev.* **2003**, *32*, 276.

(4) Furukawa, H.; Müller, U.; Yaghi, O. M. "Heterogeneity within orde" in metal-organic frameworks. *Angew. Chem. Int. Ed. Engl.* **2015**, *54*, 3417–30.

(5) Li, J.-R.; Kuppler, R. J.; Zhou, H.-C. Selective gas adsorption and separation in metal-organic frameworks. *Chem. Soc. Rev.* **2009**, *38*, 1477–1504.

(6) Li, J., Jian Rongand Sculley; Zhou, H.-C. Metal Organic Frameworks for Separations. **2012**, 869–932.

(7) Kärger, J.; Caro, J.; Cool, P.; Coppens, M.-O.; Jones, D.; Kapteijn, F.; Rodríguez-Reinoso, F.; Stöcker, M.; Theodorou, D.; Vansant, E. F. et al. Benefit of Microscopic Diffusion Measurement for the Characterization of Nanoporous Materials. *Chem. Eng. Technol.* **2009**, *32*, 1494–1511.

(8) Davis, M. E. Ordered porous materials for emerging applications. *Nature* **2002**, *417*, 813–821.

(9) Stallmach, F.; Gröger, S.; Künzel, V.; Kärger, J.; Yaghi, O. M.; Hesse, M.; Müller, U. NMR studies on the diffusion of hydrocarbons on the metal-organic framework material MOF-5. *Angew. Chem. Int. Ed. Engl.* **2006**, *45*, 2123–6.

(10) Kolokolov, D. I.; Diestel, L.; Caro, J.; Freude, D.; Stepanov, A. G. Rotational and Translational Motion of Benzene in ZIF 8 Studied by 2 H NMR: Estimation of Microscopic Self-Di ff usivity and Its Comparison with Macroscopic Measurements. **2014**, 4–10.

(11) Schlayer, S.; Pusch, A.-K.; Pielenz, F.; Beckert, S.; Peksa, M.; Horch, C.; Moschkowitz, L.; Einicke, W.-D.; Stallmach, F. X-Nuclei NMR Self-Diffusion Studies in Mesoporous Silica Foam and Microporous MOF CuBTC. *Materials (Basel).* **2012**, *5*, 617–633.

(12) Pusch, A.-K.; Splith, T.; Moschkowitz, L.; Karmakar, S.; Biniwale, R.; Sant, M.; Suffritti, G. B.; Demontis, P.; Cravillon, J.; Pantatosaki, E. et al. NMR studies of carbon dioxide and methane self-diffusion in ZIF-8 at elevated gas pressures. *Adsorption* **2012**, *18*, 359–366.

(13) Chmelik, C.; Freude, D.; Bux, H.; Haase, J. Ethene/ethane mixture diffusion in the MOF sieve ZIF-8 studied by MAS PFG NMR diffusometry. *Microporous Mesoporous Mater.* **2012**, *147*, 135–141.

(14) Sholl, D. S.; Lively, R. P. Seven chemical separations to change the world. *Nature* **2016**, *532*, 435.

(15) Alaerts, L.; Maes, M.; Jacobs, P. A.; Denayer, F. M.; Vos, D. E. D. Activation of the metal – organic framework MIL-47 for selective adsorption of xylenes and other difunctionalized aromatics. *Phys. Chem. Chem. Phys.* **2008**, *10*, 2979–2985.

(16) Rives, S.; Jobic, H.; Kolokolov, D. I.; Gabrienko, A. A.; Stepanov, A. G.; Ke, Y.; Frick, B.; Devic, T.; Maurin, G. Diffusion of Xylene Isomers in the MIL-47(V) MOF Material: Synergic Combination of Computational and Experimental Tools. *J. Phys. Chem.* **2013**, *47*, 6293–6302.

(17) Gabrienko, A.; Frick, B. Diffusion of Xylene Isomers in the MIL-47 (V) MOF Material : A Synergic Combination of Synergic Combination of Computational and Experimental Tools. *J. Phys. Chem. C* **2013**, *47*, 6293–6302.

(18) Moreira, M. A.; Santos, C.; Ferreira, A. F. P.; Loureiro, M. Influence of the Eluent in the MIL-53 (Al) Selectivity for Xylene Isomers Separation. *Ind. Eng. Chem. Res.* **2011**, *50*, 7688–7695.

(19) Duan, L.; Dong, X.; Wu, Y.; Li, H.; Wang, L.; Song, L. Adsorption and diffusion properties of xylene isomers and ethylbenzene in metal–organic framework MIL-53 (Al). *J. Porous Mater.* **2013**, *53*, 431–440.

(20) Alaerts, L.; Kirschhock, C. E. a.; Maes, M.; van der Veen, M. a.; Finsy, V.; Depla, A.; Martens, J. a.; Baron, G. V.; Jacobs, P. a.; Denayer, J. F. M. et al. Selective adsorption and separation of xylene isomers and ethylbenzene with the microporous vanadium(IV) terephthalate MIL-47. *Angew. Chem. Int. Ed. Engl.* **2007**, *46*, 4293–7.

(21) Finsy, V.; Verelst, H.; Alaerts, L.; De Vos, D.; Jacobs, P. a.; Baron, G. V.; Denayer, J. F. M. Pore-filling-dependent selectivity effects in the vapor-phase separation of xylene isomers on the metal-organic framework MIL-47. *J. Am. Chem. Soc.* **2008**, *130*, 7110–8.

(22) Gu, Z.-y.; Jiang, D.-q.; Wang, H.-f.; Cui, X.-y.; Yan, X.-p. Adsorption and Separation of Xylene Isomers and Ethylbenzene on Two Zn-Terephthalate Metal-Organic Frameworks. *J. Phys. Chem. C* **2010**, *114*, 311–316.

(23) Gee, J. a.; Sholl, D. S. Effect of Framework Flexibility on C 8 Aromatic Adsorption at High Loadings in Metal–Organic Frameworks. *J. Phys. Chem. C* **2016**, *120*, 370–376.

(24) Germanus, a.; Kärger, J.; Pfeifer, H.; Samulevič, N.; Zdanov, S. Intracrystalline self-diffusion of benzene, toluene and xylene isomers in zeolites NaX. *Zeolites* **1985**, *5*, 91–95.

(25) Trens, P.; Belarbi, H.; Shepherd, C.; Gonzalez, P.; Ramsahye, N. A.; Lee, U. H.; Seo, Y. K.; Chang, J. S. Adsorption and separation of xylene isomers vapors onto the chromium terephthalate-based porous material MIL-101(Cr): An experimental and computational study. *Microporous Mesoporous Mater.* **2014**, *183*, 17–22.

(26) Moreira, M. A.; Santos, C.; Ferreira, A. F. P.; Loureiro, J. M.; Ragon, F.; Horcajada, P.; Shim, K.-e.; Hwang, Y.-k.; Lee, U.; Chang, J.-s. et al. Reverse Shape Selectivity in the Liquid-Phase Adsorption of Xylene Isomers in Zirconium Terephthalate MOF UiO-66. *Langmuir* **2012**, *21*, 5715–5723.

(27) Braun, E.; Chen, J. J.; Schnell, S. K.; Lin, L.-C.; Reimer, J. a.; Smit, B. Nanoporous Materials Can Tune the Critical Point of a Pure Substance. *Angew. Chem. Int. Ed. Engl.* **2015**, *54*, 14349–52.

(28) Chen, J. J.; Kong, X.; Sumida, K.; Manumpil, M. A.; Long, J. R.; Reimer, J. a. Ex Situ NMR Relaxometry of Metal-Organic Frameworks for Rapid Surface-Area Screening. *Angew. Chemie Int. Ed.* **2013**, n/a–n/a.

(29) Carr, H.; Purcell, E. Effects of Diffusion on Free Precession in Nuclear Magnetic Resonance Experiments*. *Phys. Rev.* **1954**, *94*, 630–638.

(30) Casanova, F.; Perlo, J. In *Single-Sided NMR*; Casanova, F., Perlo, J., Blümich, B., Eds.; Springer Berlin Heidelberg: Berlin, Heidelberg, 2011.

(31) Galvosas, P.; Callaghan, P. T. Multi-dimensional inverse Laplace spectroscopy in the NMR of porous media. *Comptes Rendus Phys.* **2010**, *11*, 172–180.

(32) Plimpton, S. Fast Parallel Algorithms for Short – Range Molecular Dynamics. *J. Comput. Phys.* **1995**, *117*, 1–42.

(33) Nosé, S. A molecular dynamics method for simulations in the canonical ensemble. *Mol. Phys.* **1984**, *52*, 255–268.

(34) Hoover, W. G. Canonical dynamics: Equilibrium phase-space distributions. *Phys. Rev. A* **1985**, *31*, 1695–1697.

(35) Kamberaj, H.; Low, R. J.; Neal, M. P. Time reversible and symplectic integrators for molecular dynamics simulations of rigid molecules. *J. Chem. Phys.* **2005**, *122*, 224114.

(36) Dubbeldam, D.; Walton, K. S.; Ellis, D. E.; Snurr, R. Q. Exceptional Negative Thermal Expansion in Isoreticular Metal- Organic Frameworks. *Angew. Chem. Int. Ed.* **2007**, *46*, 4496–4499.

(37) Wick, C. D.; Martin, M. G.; Siepmann, J. I. Transferable Potentials for Phase Equilibria. 4. United-Atom Description of Linear and Branched Alkenes and Alkylbenzenes. *J. Phys. Chem. B* **2000**, *104*, 8008–8016.

(38) Ford, D. C.; Dubbeldam, D.; Snurr, R. Q.; Snurr, R. Q. The Effect of Framework Flexibility on Diffusion of Small Molecules in the Metal-Organic Framework IRMOF-1. *Open-Access J. Basic Princ. Diffus. Theory, Exp. Appl.* **2009**, *11*, 1–8.

(39) Lemak, A. S.; Balabaev, N. K. On The Berendsen Thermostat. *Mol. Simul.* **1994**, *13*, 177–187.

(40) Frenkel, D.; Smit, B. *Understanding Molecular Simulation: From Algorithms to Applications, Elzevier Science 2002*; 2002.

(41) Dubbeldam, D.; Ford, D.; Ellis, D.; Snurr, R.; Dubbeldam, D.; Ford, D.; Ellis, D.; Snurr, R.; Perspective, A. N. A New perspective on the Order-n Algorithm for Computing Correlation Functions. *Mol. Simul.* **2009**, *35*, 1084–1097.

(42) Mazza, M. G.; Giovambattista, N.; Stanley, H. E.; Starr, F. W. Connection of translational and rotational dynamical heterogeneities with the breakdown of the Stokes-Einstein and Stokes-Einstein-Debye relations in water. *Physical Review E* **2007**, *76*, 031203.

(43) Rousseau, B.; Petravic, J. Transport coefficients of xylene isomers. *The Journal of Physical Chemistry B* **2002**, *106*, 13010–13017.

(44) Kitchlew, A.; Rao, B. D. N. Temperature dependence diffusion in liquids. *Mol. Phys.* **1971**, *21*, 1145–1147.

(45) L. Sudmeier, J.; E. Anderson, S.; S. Frye, J. Calculation of Nuclear Spin Relaxation Times. *Concepts Magn. Reson.* **1990**, *2*, 197–212.

(46) Kowalewski, J.; Maler, L. *Nuclear Spin Relaxation in Liquids: Theory, Experiments, and Applications*; 2006.

(47) Szabo, A. Model-Free Approach to the Interpretation of Nuclear Magnetic Resonance Relaxation in Macromolecules . 1 . Theory and Range of Validity. *J. Am. Chem. Soc.* **1982**, *104*, 4546–4559.

(48) Andrec, M.; Montelione, G. T.; Levy, R. M. Lipari – Szabo mapping : A graphical approach to Lipari – Szabo analysis of NMR relaxation data using

reduced spectral density mapping. *J. Biomol. NMR* **2000**, *18*, 83–100.

(49) Kimmich, R. Strange kinetics, porous media, and NMR. *Chem. Phys.* **2002**, *284*, 253–285.

(50) Eades, R. G.; Jones, T.; Llewellyn, J. P. N.M.R. Investigation of Molecular Motions in Solid Xylene. *J. Chem. Soc. Faraday Trans. 2 Mol. Chem. Pysics* **1972**, 1316–1322.